Cannabinoids shift the basal ganglia miRNA m^{6}A methylation profile towards an anti-inflammatory phenotype in SIV-infected Rhesus macaques

Chioma M. Okeoma[1,2]*, Lakmini S. Premadasa[3], Chen S. Tan[4], Ionita C. Ghiran[5*], Mahesh Mohan[3*]

[1]Department of Pathology, Microbiology & Immunology, New York Medical College, Valhalla, NY, USA

[2]Lovelace Biomedical Institute, Albuquerque, NM 87108-5127, USA.

[3]Southwest National Primate Research Center, Texas Biomedical Research Institute, San Antonio, TX 78227-5302, USA.

[4]Division of Infectious Diseases, Department of Internal Medicine, University of Iowa, Iowa City, IA 52242, USA

[5] Department of Anesthesia, Critical Care and Pain Medicine, Beth Israel Deaconess Medical Center, Harvard Medical School, Boston, MA, USA

*Correspondence: cokeoma@nymc.edu; ighiran@bidmc.harvard.edu, MMohan@txbiomed.org

Highlights

- SIV infection induced significant m^{6}A modification changes in basal ganglia (BG) miRNA.
- m^{6}A hypomethylated miRNAs are abundant in BG tissues of infected rhesus macaques (RM).
- m^{6}A epitranscriptomic marks in BG miRNAs of infected RMs are linked to neuroinflammation network genes.
- BG tissue miRNAs with m^{6}A epitranscriptomic marks are present in BG-derived Extracellular Vesicles (EVs).
- Target genes of EV-Tissue miRNAs with m^{6}A epitranscriptomic marks have diverse predictive functions.

Summary

Epitranscriptomic modifications modulate diverse biological processes, such as regulation of gene expression, abundance, location and function. In particular, N6-methyladenosine (m^{6}A) methylation has been shown to regulate various disease processes, including cancer and inflammation. While there is evidence that m^{6}A modification is functionally relevant in neural development and differentiation, the role of m^{6}A modification in HIV neuropathogenesis is unknown. Here, we identified direct m^{6}A modifications in miRNAs from BG tissues of

Rhesus macaques (RMs) that were either vehicle-treated uninfected (VEH), SIV-infected and combination anti-retroviral therapy (cART) and VEH treated (VEH/SIV/cART), or THC:CBD treated (THC:CBD/SIV/cART). We detected m^6A modifications across all three treatment groups. SIV infection promoted an overall hypomethylated m^6A profile. While the overall hypomethylated m^6A profile was not significantly impacted by THC:CBD treatment, specific miRNAs, particularly those predicted to target proinflammatory genes showed markedly reduced m^6A methylation levels compared to the VEH treated RMs. Additionally, we found that specific BG tissue miRNAs bearing m^6A epi-transcriptomic marks were also transferred and detected in BG-derived extracellular vesicles (EVs). Mechanistically, we identified the DRACH motif of the seed region of miR-194-5p to be significantly m6A hypomethylated, which was predicted to directly target STAT1, an important interferon-activated transcription factor known to drive neuroinflammation, in diseases ranging from Alzheimer's to Parkinson's and Huntington's disease. Notably, THC:CBD treatments significantly reduced m^6A methylation of 44 miRNA species directly involved in regulating CNS network genes, thus providing a possible mechanistic explanation underlying the beneficial effects of THC:CBD in several diseases involving neuroinflammation. Our findings also underscore the need for investigating the qualitative, and posttranscriptional modifications in RNA along with the more traditional, quantitative alterations in pathological conditions or in response to disease modifying treatments.

Keywords

N6-methyladenosine (m^6A), epitranscriptomic marks, post-transcriptional RNA modification, SIV, neuroinflammation network genes.

Introduction

Despite successful control of HIV with combined antiretroviral therapy (cART)(1-3), up to 50% of persons living with HIV (PLWH) still suffer from HIV Associated Neurocognitive Disorders (HAND)(4, 5). A major factor driving HAND is considered to be incomplete viral suppression in the CNS, and the consequent activation of resident microglia, leading to neuroinflammation and neuronal damages.

In addition, drug abuse is a major comorbidity, where ~40% of PLWH use cocaine andcannabis(6-9), resulting in increased virus-induced pathology(10-15), though cannabis use could afford varying degrees of protection from immune activation/inflammation (7). While collecting longitudinal blood and matched brain samples from PLWH and healthy controls is extremely challenging, the availability of the SIV-infected RM model supports investigation of phytocannabinoids and other drugs of abuse on HIV/SIV neurological disease progression and has the potential to shed light on the underlying molecular mechanisms. Our previous studies, using the non-human primate (NHP) model, showed that twice daily administration of low-dose delta-9-tetrahydrocannabinol (THC) to RMs significantly reduced expression of type I-interferon (IFN) induced genes including inflammation associated miRNAs, miR-155 and miR-142-3p, in basal ganglia (BG) of cART naïve SIV-infected RMs(16, 17). The effect of THC on BG was also present in BG-derived extracellular vesicles (EVs)[8]. Transcriptomic analyses of miRNAs associated with EVs isolated from these BG tissues revealed that both SIV infection and THC administration induced distinct but significant changes in BG EV-associated miRNAs, which were predicted to regulate pathways related to inflammation/immune regulation, TLR signaling, neurotrophin TRK receptor signaling, and cell death/response(18). Long-term administration of low-dose THC to SIV infected RMs led to significant upregulation of 37 miRNAs in BG-EVs. Of these 37 miRNAs, 11 miRNAs were significantly downregulated in EVs from SIV infected control RMs that received vehicle control instead of THC.

Recent studies have identified over 170 RNA modifications, among which, m^6A (N6-methyladenosine) is the most abundant modification in mammalian RNA, occurring in ~50% of the total methylated ribonucleotides(19). RNA m^6A modifications regulate a wide variety of processes such as metabolism, splicing, translation, and degradation of RNA as well as in disease pathogenesis. m^6A modifications have been described not only in mRNA but also recently in miRNAs, a class of small noncoding regulatory RNAs. miRNAs play key roles in regulating protein translation and has been implicated in various neurological disorders, including cognitive impairment. While others and we have published the role of miRNAs in the regulation of gene expression in the brain, there is a significant knowledge gap regarding the role of post transcriptional changes, in particular, miRNA m^6A modification and its implications in HIV/SIV neuropathogenesis. Accordingly, the present study investigated the relationship between HIV/SIV infection of BG, miRNA m^6A alterations, and the potential impact of concurrent phytocannabinoid use on miRNA m^6A modifications and its potential implications for HAND pathogenesis.

Here, we present data supporting shifts in the small RNA landscape in the BG in response to HIV/SIV infection and cART treatment and the impact of concurrent THC:CBD administration. In addition to changes in the expression levels of several miRNA species involved in cognition and neuroinflammation, we also detected for the first-time significant alterations in the m^6A methylation levels of key miRNA species, suggesting an added, more refined level of protein expression control. By exploring the interplay involving HIV/SIV infection, miRNA m^6A alterations in BG, and phytocannabinoid use, this study aims to offer a comprehensive understanding of the role of m^6A modifications on miRNA function that may provide valuable mechanistic insights into the development of HAND and pave the way for novel therapeutic strategies to mitigate cognitive decline in PLWH.

Results

Quantification of m^6A profiles of BG miRNAs point to mechanistically relevant species involved in the anti-inflammatory effect of THC:CBD treatment. Altered m6A-modified RNAs expression levels in the brain were linked to dysregulation of key genes involved in immune cell activation, cytokine production, and blood-brain barrier integrity, which could modulate the activation of microglia and astrocytes, thereby, initiating and exacerbating neuroinflammatory processes(20, 21). Most of the published research regarding the role of m6A changes in neuroinflammation has centered on mRNA and lncRNA and not miRNA molecules (reviewed in(22). Hence, we focused exclusively on miRNAs in the present study.

All seven SIV-infected RMs, receiving either VEH (n=4) or THC:CBD (n=3), had substantial plasma viral loads ranging from 1.93 to 16.8 x 10^6 copies/mL during acute infection [12-20 days post SIV infection (DPI)] (**Table 1**). However, cART initiation at 30 DPI effectively suppressed viral replication, as viral RNA was undetectable in both plasma and BG at necropsy (180 DPI).

We investigated how SIV infection and/or THC:CBD altered the landscape of m^6A changes in miRNAs isolated from BG of RMs that were either i) uninfected (Control), ii) SIV-infected treated with cART and administered either vehicle (VEH) alone (VEH/SIV/cART), or iii) SIV-infected, treated with cART and administered THC:CBD (THC-CBD/SIV/cART). The m6A analyses were performed by microarray hybridization profiling following pull down of m^6A modified miRNAs using an m^6A specific antibody (Synaptic Systems). BG tissues from all three groups were analyzed for miRNA m^6A modifications. After quality control and filtering, we used a p-value (unpaired t-test) <= 1.0 and fold-change >= 0.0 to identify a total of 1805 miRNAs that were m^6A modified in all

experimental groups irrespective of statistical significance (**Supplemental Table 1**). We compared each treatment group to the uninfected control group and found that SIV infection induced a significantly broader m^6A hypomethylation of BG miRNAs (**Table 2**) compared to hypermethylation. Of the total 1805 miRNAs in the VEH/SIV/cART group with m^6A modifications, 1281 (71%) were mature miRNAs, while 524 (29%) were passenger strand (PS) miRNAs (generated from the opposite (3') strand) (**Fig. 1A**). Over 95% of the mature and PS miRNAs were m^6A hypomethylated in VEH/SIV/cART (**Fig. 1B**) and in THC:CBD/SIV/cART (**Fig. 1C**) RMs compared to uninfected controls (**Figs. 1B, 1C**). In contrast, only 6% and 5% of mature and PS miRNAs, respectively, were hypomethylated when comparing VEH/SIV/cART to THC:CBD/SIV/cART (**Fig. 1D**) RMs. Raw intensities of IP of m^6A- and unmodified-miRNA species, respectively, were normalized with average of log2-scaled Spike-in RNA intensities. We found an overall inverse relationship between m^6A methylation and expression abundance of the miRNA species in VEH/SIV/cART (**Fig. 1E**) and THC:CBD/SIV/cART (**Fig. 1F**) RMs when compared to controls, and that of VEH/SIV/cART when compared to THC:CBD/SIV/cART (**Fig. 1G**) RMs. Our data presented above show that while unsupervised clustering of the differentially expressed miRNAs species isolated from BG fails to separate the control from the THC:CBD treated group, analyses of the differentially m6A-modified miRNA clearly identifies changes in the miRNA profile promoted by the THC:CBD treatments, underscoring the need for functional quantification of the RNA levels in addition to the canonical up and down quantifications.

SIV infection increased the overall m^6A methylation levels in BG-derived miRNAs. Further analyses of the m^6A methylated miRNAs were conducted to identify significantly m^6A modified miRNAs using p-value < 0.05 (unpaired t-test) and fold change >= 1.5. We found that most of the m^6A modified miRNAs were present in mature miRNAs with percentages ranging from 60 to 72% (**Figs. 2A-F**). While SIV infection induced significant hypo m^6A modifications in BG miRNAs in over 1000 miRNA species when compared to control animals, hypermethylation changes were identified in only seven miRNA species (**Table 3**). We next compared methylation levels with miRNA abundance (expression), by calculating the miRNA abundance using mean m^6A RNA modification quantity per treatment, mean m^6A RNA modification quantity for control, and the difference of mean percentage of m^6A RNA modification (%Modified) between the treatment and control groups. The levels of the m^6A modification versus abundance are displayed as heatmaps (**Figs. 2G-L**). The top 5 miRNAs or fewer

(depending on the group) were selected and their m^6A and expression levels are presented as heatmaps (**Figs. 2M-R**).

Pathway analysis of SIV-induced m^6A epitranscriptomic marks in BG miRNAs of SIV-infected RMs identified top neuroinflammation network genes:

To analyze the biological implications of m^6A-enriched miRNAs, we used ingenuity pathway analysis (IPA) to perform enrichment analysis of predicted and validated genes (**Supplemental Table 1**) targeted by hypo or hyper m^6A methylated miRNAs using criteria determined apriori. We identified neuroinflammation network genes associated with the miRNAs from each group that were hypomethylated (**Supplemental Fig. 1 left, Fig. 3A**) or hypermethylated (**Supplemental Fig. 1 right, Fig. 3B**). The top 35 IPA neuroinflammation network genes associated with m^6A hypo and hyper methylated miRNAs are shown in **Table 4**. In addition to the protein networks altered by the methylated miRNAs, our results also identified several miRNA species which were also targeted by the m6A-modified miRNAs. These data are consistent with previous reports that demonstrated regulation of primary miR-21 by mature miR-122 (23-25).

Integration of IPA and GO analyses. Our analyses identified several disease-related functional clusters linked to neuroinflammation network genes associated with m^6A hypo and hyper methylated miRNAs (**Table 5**). Whereas the top three diseases related to changes in invasion, migration, and proliferation of cells, were linked to a hypomethylated m^6A profile (rows 1-4), diseases associated with changes in quantity of cells, organization of cytoskeleton, and neurotransmission were linked to the hypermethylated m^6A profile (rows 1-3). Integration of IPA and the 35 neuroinflammation genes with WEB-based Gene SeT Analysis Toolkit (WebGestalt) GO analysis identified several biological processes, cellular components, and molecular functions of the neuroinflammation network genes for each group that stratified into targets of hypomethylated m^6A (**Fig. 4A**) and hypermethylated m^6A (**Fig. 4B**).

Conjoint Analysis of m^6A methylation and differentially altered miRNA expression. We determined the functional significance of m^6A methylation of miRNAs, by first determining the relative abundance of the m^6A hypo and hyper methylated miRNAs species. After obtaining the abundance of miRNAs with significant m^6A

modifications, we found that majority of significantly m^6A-modified miRNAs were either significantly up or down regulated (**Table 6**). We also found a positive correlation between m^6A methylation and miRNA abundance for Hypo_VEH/SIV/cART_vs_Controls (Pearson r=0.72; p<1e-10) and Hypo_THC:CBD/SIV/cART_vs_Controls (Pearson r=0.84; $p<1e^{-10}$) (**Figs. 5A, 5B)**, respectively. However, we did not identify any additional correlations among other treatment groups (**Supplemental Fig. 2**). To examine the functional relationship of m^6A methylated miRNAs, we used IPA miRNA Target Filter focused on miRNAs related to neurotransmitter networks and nervous system-centered signaling pathways (**Figs. 5C-H, Table 7**). Analysis of protein:protein interactions (PPI) for the IPA identified miRNA targets using STRING: functional protein association networks (*https://string-db.org/*) led to the identification of several gene clusters and nodes associated with the m^6A methylation status (hypermethylation vs hypomethylation) and miRNA abundance that may shed light into the potential biological functions of miRNA m^6A methylation (**Figs. 5I-N**). The potential biological functions of the miRNA targets were further revealed by GO biological processes, molecular functions, cellular components, Kegg/Reactome/Wiki pathways, disease gene associations, and tissue expressions (**Table 8**).

THC:CBD administration significantly reduced the m^6A levels in the seed sequence of HIV/SIV-altered miRNAs regulating neuroinflammation. Relative to the THC:CBD/SIV/cART group,44 miRNAs showed significant m^6A hypermethylation in the VEH/SIV/cART RMs (**Fig. 6A**). More importantly, IPA analyses of the genes targeted by the 44 miRNAs that were hypermethylated in BG of VEH/SIV/cART compared to THC:CBD/SIV/cART RMs (**Table 8**) identified neuroinflammation gene networks previously shown to drive neuroinflammation, neuropathogenesis of Huntington's, Alzheimer's, Parkinson's diseases, (**Fig. 6B**). Key biological processes regulated by these m^6A hypermethylated miRNAs included gamma-aminobutyric acid signaling pathway, synaptic transmission, cognition, immune-response regulating signaling pathway and positive regulation of cytokine production (**Fig. 6C**). GABA receptor activity, glutamate receptor activity, neurotransmitter receptor activity, gated channel activity, cytokine receptor activity were the most significant molecular functions enriched for these mRNA targets. Additionally, the targets of the miRNAs associated with KEGG are linked to GABAergic synapse, leishmaniasis, and nicotine addiction. Reactome pathways are linked to Toll-like receptor 5 cascade, MyD88 cascade, neurotransmitter receptors and postsynaptic signal transmission, signaling by interleukins, and cytokine signaling in the immune system. Diseases associated with autistic disorder, asthma

reperfusion injury, atherosclerosis, substance withdrawal syndrome, nerve degeneration, cholestasis, myocardial reperfusion injury, urticaria, hepatic encephalopathy (**Supplemental Figs. 2A-C**). Further analysis of the 44 m^6A hypermethylated miRNA revealed RRACH or DRACH motif in 14 out of the 44 miRNAs (**Table 9**), indicating that the rest of the m6A methylation events took place in non-canonical DRACH motives(26). IPA network linked the targets of the 14 miRNAs with RRACH or DRACH motif to canonical signaling pathways of NF-kB activation by viruses, neuroinflammation signaling, and transcriptional activity by SMAD heterotrimer, all of which are functionally linked to cognitive impairment(27-29) (**Fig. 6D**).

Basal ganglia tissue miRNAs enriched in m^6A modification are also present in basal ganglia-derived Extracellular Vesicles (EVs). We integrated BG tissue miRNA abundance with miRNA counts from our previously published BG derived EVs (BG EVs) miRNA sequence dataset (18) to identify tissue miRNAs with m^6A modifications that were also present in the BG EVs dataset. Of the 527 miRNAs identified in EVs from the BG of SIV infected RMs, 162 (11.1%) were also present in RM whole BG tissues (**Fig. 7A**). Although methylation analyses were not conducted on the EV derived miRNAs, all 162 miRNAs were m^6A hypomethylated in the BG tissues and none of the m^6A hypermethylated miRNAs were present in EVs, suggesting either a sorting mechanism based on the methylation status of the miRNAs, or an active de-methylation process performed by m6A erasers, which may be present in EVs (**Fig. 7A**). The top 5 EV-associated miRNAs belonged to the let-7 family (let-7a-5p, let-7c-5p, let-7b-5p, miR-26a-5p, let-7f-5p) (**Fig. 7B**) and were different from the top 5 (miR-320b, miR-504-3p, miR-1224-5p, miR-372-3p, miR-193b-5p) miRNAs found in BG tissues (**Fig. 7C**). Next, we used IPA to identify target genes of the 162 BG tissue-EVs miRNAs that were linked to neuroinflammation canonical pathways (**Fig. 7D**). The target genes were used to predict protein-protein interactions to gain insight into potential direct (physical) and indirect (functional) associations. Three gene clusters were identified (**Fig. 7E**). Their predicted GO Biological Processes detected included processes related to uterine wall breakdown, negative regulation of interleukin-23 production, positive regulation of EMT involved in endocardial cushion formation, positive regulation of tight junction disassembly, positive regulation of additional functions and signaling pathways (**Table 10).** Furthermore, we used WebGestalt to translate the 162 tissue-EV miRNA target gene lists into biological/functional insights using over representation analyses (ORA) with the Benjamini-

Hochberg procedure aimed at reducing the false discovery rate and avoiding type I errors. Ten functional categories were enriched, including neuron death, positive regulation of response to external stimulus, leukocyte proliferation, positive regulation of cell motility, regulation of leukocyte, response to molecule of bacterial origin, T cell activation, regulation of cell-cell adhesion, positive regulation of cell activation, extrinsic apoptotic signaling pathway (**Fig. 6F**). The gene list involved in each of the functional categories is presented in **Table 11**.

Discussion:

Despite the widespread application of multi-omics (mRNA, microRNA and LncRNA profiling) technologies to understanding the pathogenesis of HAND, the field of "epi-transcriptomics" involving post-transcriptional regulation of gene expression via RNA modifications and editing that impacts RNA folding, stability and interaction with its targets remains an underexplored and understudied topic in HIV/SIV infection. Except for a few *in vitro* reports, there exists a dearth of knowledge about m^6A modifications, the most researched epitranscriptomic modification of eukaryotic RNAs in host–HIV interactions. Moreover, the presence of m^6A modifications in small RNAs, such as microRNAs (miRNA), and how HIV infection modulates m^6A modifications in miRNAs during infection is unknown and unexplored. We have previously described the role of miRNAs (both tissue and extracellular vesicle derived) in HIV/SIV induced neuroinflammation and its modulation by long-term low-dose phytocannabinoids. Accordingly, to address this knowledge gap, here, we investigated the profile of BG m^6A methylome in host miRNAs during HIV/SIV infection and the potential effects of phytocannabinoids (THC and CBD) on the BG miRNA m^6A methylome. We used a combination of THC and CBD (1:3) because findings from clinical studies have confirmed that THC is well-tolerated when administered in combination with CBD(30-32). Specifically, CBD diminished the adverse effects of THC, such as tachycardia, intoxication, and sedation, while preserving the beneficial effects of reduced muscle spasticity and neuroinflammation (30-32).

We detected m^6A modifications of miRNAs from BG tissues of all RMs, irrespective of infection or long-term treatment with low-dose phytocannabinoids (THC:CBD). Interestingly, miRNAs from BG tissues of VEH/SIV/cART and THC:CBD/SIV/cART RMs bore significant hypomethylated m^6A profile compared to uninfected control (VEH) RMs with predictive link to neuroinflammation network genes. The potential functional impact of m^6A methylation on miRNA function became clearer when we performed a pathway analysis (IPA) of

the genes targeted by the 44 miRNAs that were hypermethylated in BG of VEH/SIV/cART compared to THC:CBD/SIV/cART RMs (**Table 2)**. Hypermethylation of miRNA adenine nucleotides in or near the miRNA seed region (nucleotide positions 2 to 7 in the 5' seed region) can lead to loss of target mRNA 3' UTR binding and repression(33). Therefore, in a neuroinflammatory disease like HIV/SIV infection, miRNA m^6A hypermethylation could lead to enhanced proinflammatory gene expression and disease progression. IPA processing of the target genes identified numerous neuroinflammatory genes such as STAT1, CCL2, CXCL12, IFNA4, TIRPA, NOS2, IL6R, IL34, all known to promote neuroinflammation and drive progression of numerous neurological diseases such as Huntington's, Alzheimer's, and Parkinson's disease, (Fig 5). Interestingly, others(34) and we(17) have also shown significant upregulation of expression of type-I IFN stimulated genes in the brains of SIV-infected RM. To the best of our knowledge, we provide the first evidence of the presence of m^6A modifications with a shift towards significant m^6A hypomethylation in mature miRNAs in the brain during HIV/SIV infection.

The presence of m^6A modified mature miRNAs was recently reported in HEK293T(35), human lung cancer cells, and fibroblast cells in response to hypoxia(33, 36). Here, using the SIV-infected RM model, we profiled and identified differential m^6A methylation in both mature and PS miRNAs in whole BG tissues, although majority of the m^6A modified miRNAs detected originated from the mature strand. While SIV infection triggered a significant hypomethylated profile in BG tissue miRNAs, miRNA expression abundance was inversely correlated to m^6A methylation in VEH/SIV/cART and THC:CBD/SIV/cART RMs compared to controls RMs. We also identified a set of BG tissue miRNAs [(n=162) ~11.1%] with m^6A epitranscriptomic marks that were also present in BG EVs(18) (**Figure 6**). All 162 BG tissue-EV miRNAs that bore m^6A marks were hypomethylated and none were hypermethylated.

Next, we used IPA and WebGestalt to predict the potential functional relevance of m^6A modified miRNAs. Interestingly, miRNAs bearing m^6A marks were found to have a link to neuroinflammation network genes, neurotransmitters/other nervous system, and pathogen influenced signaling pathways. The top three functional classifications included invasion, migration, and proliferation of cells in generalized disease states linked to m^6A hypomethylation profile while quantity of cells, organization of cytoskeleton, neurotransmission were the

important functional groups/processes found to be linked to the hypermethylated m^6A profile (**Table 4**). PPI predicted functions and signaling pathways of BG tissue m^6A-enriched miRNAs that were also present in BG EVs, revealed GO biological processes that included negative regulation of interleukin-23 production, positive regulation of EMT involved in endocardial cushion formation, positive regulation of tight junction disassembly, and positive regulation of calcidiol 1-monooxygenase activity (**Table 8**), all with potential relevance to HIV/SIV induced neurological disease. Recent studies have shown that m^6A hypermethylation in the seed regions of mature miRNAs resulted in loss of target mRNA recognition, binding, and translational inhibition(33). Accordingly, based on these predicted functions, it is plausible that the generalized m^6A hypomethylation may be a host response to enable m^6A hypomethylated miRNAs to successfully regulate the expression of proinflammatory mediators, such as IL-23, STAT1, NOS1, and the blood brain barrier integrity by promoting posttranscriptional gene silencing.

Although SIV infection decreased m^6A modifications of BG tissue miRNAs, Lichinchi et al., found that in T cells, HIV infection increased m^6A marks in both host and viral mRNAs (37). Altogether, our findings show that BG miRNA m^6A modifications may play important roles in host–HIV interactions, as previously suggested in other viral infections, although those studies focused entirely on mRNAs (37-39) and not miRNAs.

From a functional perspective, m^6A miRNA modifications in BG tissues may represent a potential mechanism to regulate host miRNA dependent regulation of proinflammatory gene expression that may impact HIV neuropathogenesis. This is clear from recent studies showing m6A methylation of the adenine residue/s in miR-21-5p(33), where m6A modification of adenine residues near the seed region resulted in loss of target gene (MAPK10 and PTEN) repression in A549 cells. Therefore, the significantly reduced m^6A methylation in 44 neuroinflammatory gene targeting miRNAs in the THC:CBD/SIV/cART compared to the VEH/SIV/cART group suggests that cannabinoids may preserve the post-transcriptional gene regulatory functions of anti-inflammatory miRNAs by reducing their m^6A epitranscriptomic marks. Our recently published studies found long-term low-dose THC administration to significantly reduce type I-interferon stimulated gene expression(17). Since type-I IFNs activate STAT1(40), we performed bioinformatics analysis using TargetScan 8.0 and identified RM STAT1 to be a predicted target of miR-194-5p with a perfect match between the seed sequence of miR-194-5p and the

3' UTR region of STAT1 (**Supplemental Fig. 4**). Interestingly, miR-194-5p showed markedly more hypomethylation in THC:CBD/SIV/cART compared to control RMs. Increased STAT1 activated by interferons (IFN) can drive persistent neuroinflammatory signaling in a variety of neurological diseases. In addition, significant upregulation of IFN-stimulated STAT1 protein expression in the brain has been confirmed by others in the SIV-infected RM model(34). We further identified a DRACH motif (where, D= A, G or U; U, R= A or G, and H=A, C or U) in the seed region (nucleotides 2-7 from the 5' end) of miR-194-5p (5'-UG**UAA*CA**GC**AACU**CCAUGUGGA-3').

Overall, our in silico findings suggest that reduced m^6A methylation of miR-194-5p is expected to preserve its target binding capacity and may represent a potential posttranscriptional gene silencing mechanism by which THC or THC:CBD may reduce STAT1 expression. Under in vitro conditions, m^6A methylation of adenine residues in mature miRNAs resulted in reduced suppression of target gene expression, suggesting that m^6A modification of miRNA seed nucleotides can interfere with mRNA target recognition and binding. Therefore, in vitro overexpression studies using miR-194-5p mimics containing m^6A methylated adenosine nucleotides in the seed region on STAT1 protein expression are needed in the future. It is possible that THC:CBD may mediate these changes through altering the expression levels of m^6A writers and erasers that catalyze the addition and removal of m^6A epitranscriptomic marks. Therefore, future studies are needed to address these knowledge gaps including whether extracellular miRNAs bear similar m^6A marks and the implications of such epitranscriptomic marks in HIV neuropathogenesis.

Material and Methods

Animal care, ethics, and experimental procedures

All experiments using RM (**Table 1**) were approved by the Texas Biomedical Research Institute's (Texas Biomed) Institutional Animal Care and Use Committee (Protocols 1734MM). The Southwest National Primate Research Center (SNPRC) is an association for Assessment and Accreditation of Laboratory Animal Care International-accredited facility (AAALAC #000246). The NIH Office of Laboratory Animal Welfare assurance number for the SNPRC is D16-00048. All clinical procedures, including administration of anesthesia and analgesics, were carried out under the direction of a laboratory animal veterinarian. Animals were pre-

anesthetized with ketamine hydrochloride, acepromazine, and glycopyrrolate, intubated and maintained on a mixture of isoflurane and oxygen. All possible measures were taken to minimize the discomfort of all the animals used in this study. Texas Biomed complies with NIH policy on animal welfare, the Animal Welfare Act, and all other applicable federal, state and local laws.

Animal model and experimental design

Twelve age and weight-matched male Indian RMs were randomly distributed into three groups (**Table 1**). Group 1 [uninfected controls (n = 4)] served as uninfected controls. Groups 2-3 (n = 38) were infected intravenously with 100 times the 50% tissue culture infective dose (100TCID$_{50}$) of SIVmac251. Group 2 [VEH/SIV/cART] (n = 4) received twice daily injections of vehicle (VEH) (1:1:18 of emulphor:ethanol:saline), intramuscularly. Group 3 [THC:CBD/SIV/cART] (n = 4) received twice daily injection of THC:CBD (1:3 ratio) intramuscularly beginning four weeks after SIV infection at 0.18mg/kg, as used in previous studies(17). This dose of THC was increased to 0.32mg/kg over a period of 2 weeks and maintained for the duration of the study. For animals in groups 2 and 3 (n = 8), cART was administered daily by subcutaneous injection and included TDF (5.1 mg/kg) (Gilead), Emtricitabine (30mg/kg) (Gilead) and Dolutegravir (3mg/kg) (ViiV Healthcare) and was initiated four weeks post-SIV infection (same time as initiation of cART or VEH injections). Basal ganglia (BG) tissue (~5cm) was collected at necropsy from all animals. A cube of 1x1x1 cm BG tissue was used for total RNA extraction. For histopathological and immunohistochemical evaluation, BG tissues were fixed in Z-fix, embedded in paraffin, sectioned at 5 μM for further analysis. SIV levels in basal ganglia were quantified using the TaqMan One-Step Real-time RT-qPCR assay that targeted the LTR gene(16). SIV inoculum, infection duration, BG viral loads, and BG histopathology is provided in **Table 1**.

Methylated RNA immunoprecipitation (MeRip):We have completed the Arraystar Human N6-methyladenosine (m6A) small RNA modification microarray analysis of the samples you submitted. The RNA samples were QC'd for quantity by NanoDrop ND-1000 spectrophotometer and RNA integrity by Bioanalyzer 2100 or gel electrophoresis. Briefly, 1-5 μg of each total RNA sample was immunoprecipitated by 4 μg anti-N6-methyladenosine antibody (Synaptic Systems) with 1 mg Protein G Dynabeads (Thermo Fisher, 11203D) in 500 μL RIP buffer. The modified RNAs were eluted from the immunoprecipitated magnetic beads as the "IP". The unmodified RNAs were recovered from the supernatant as "Sup". The "IP" and "Sup" RNAs were enzymatically

labeled with Cy5 and Cy3 respectively in separate reactions using Arraystar's standard protocols. The labeled RNAs were combined together and hybridized onto Arraystar Human small RNA Modification Microarray (8x15K, Arraystar) and the array was scanned in two-color channels by an Agilent Scanner G2505C.Agilent Feature Extraction software (version 11.0.1.1) was used to analyze the acquired array images. Raw intensities of IP (immunoprecipitated, Cy5-labelled) and Sup (supernatant, Cy3-labelled) were normalized with average of log2-scaled Spike-in RNA intensities. After normalization, the probe signals having Present (P) or Marginal (M) QC flags in at least 4 out of 12 samples were retained. Multiple probes from the same small RNA (miRNA/TsRNA (tRF&tiRNA)/pre-miRNA) were combined into one RNA level. "m6A abundance" was analyzed based on the Cy5-labelled IP (modified RNA) normalized intensities. Differentially m6A-modified RNAs between two comparison groups were identified by fold change (FC) and statistical significance (p-value) thresholds. Hierarchical Clustering heatmap was plotted to display m6A-modification patterns among samples by R software.

RNA processing and m^6A analyses: Basal ganglia tissues were collected during necropsy in 1 cm^3 cubes and processed for total RNA extraction using Qiazol (Qiagen Inc, CA). For a detailed protocol see Supplemental Information. Briefly, Total RNA was immunoprecipitated with anti-N6-methyladenosine (m6A) antibody and the modified RNAs were eluted from the beads as "m6A," and unmodified RNAs were recovered as "unmodified" samples. Raw intensities of each sample were normalized with average of log2-scaled Spike-in RNA intensities. Differentially m6A-modified RNAs between two comparison groups were identified by fold change (FC) and statistical significance (p-value) thresholds. Hierarchical Clustering heatmap was plotted to display m6A-modification patterns among samples by R software.

Criteria for selecting m^6A modified miRNA: Differentially significant m^6A methylated miRNAs were identified with p-value < 0.05, | log2(FC)| > 1 upregulation, <-1 downregulation). To identify m^6A modified miRNAs that are biologically relevant to HIV/SIV induced neuroinflammation, we used miRNA Target Filter functionality of IPA with a set of criteria to prioritize experimentally validated and predicted mRNA targets to perform enrichment analysis. Based on confidence level, diseases, cells/tissues, and pathways, we identified miRNA-mRNA, overlay miRNA data onto network pathways, and molecules. The identified miRNA target genes were fed into WEB-based GEne SeT AnaLysis Toolkit (WebGestalt, https://www.webgestalt.org/) and used for Geneontology analysis. The following criteria were used:

Tissue = Brain

Pathway = Neurotransmitters and other nervous system signaling

Disease = neurological diseases

Network overlay = neuroinflammation canonical signaling pathway. Merge multiple relevant networks.

Used IPA-generated list for STRING: functional protein association networks (https://string-db.org/) for protein:protein analysis.

Used IPA-generated list for WEB-based Gene SeT AnaLysis Toolkit (WebGestalt) GO biological, cellular, molecular processes analyses, using over representation analysis (ORA) enrichment method.

Statistical analysis: Pie Charts were generated using GraphPad Prism. Heatmaps were generated with GraphPad Prism and Heatmapper (http://heatmapper.ca/). Venn diagrams were generated with Venny 2.1 (https://bioinfogp.cnb.csic.es/tools/venny/).

Declarations:

Consent for publication: All authors read and approved the publication of this manuscript.

Competing interests: The authors report no biomedical financial interests or potential conflicts of interest.

Availability of data and materials: The dataset is included within the article and its additional files.

Funding: This work was supported by National Institutes of Health funding (Grant No. R01DA042348 [to CMO]; Grant Nos. R01DA042524 and R01 DA052845 [MM], Grant Nos. R01DA050169 and R21/R33DA053643 [to CMO & MM], R01CA218500, UH3TR002881, R01TR218500 [to IG], P30AI161943, and P51OD111033.

Author contributions: Study conceptualization and design: IG, MM and CST. CMO conducted data analyses manuscript. CMO, MM, and IG wrote the original draft, reviewed and edited the manuscript. LSP assisted with the viral load quantification, proof reading and preparation of animal information.

Figure legends:

Figure 1: Global m^6A methylation patterns basal ganglia miRNAs of RM infected with SIV and treated with THC, cART, or both THC and cART over uninfected controls: A) Percent mature and star miRNAs with m^6A methylation marks. B-D) m^6A methylation patterns in each treatment group. E-G) Heatmap of m6A methylation profile versus miRNA abundance.

Figure 2: The m6A Content of RM basal ganglia tissues was changed by SIV and THC:CBD: A-F) Pie chart representing % of mature and star miRNAs with m^6A modifications. G-L) Heatmap illustrating the levels of the m^6A methylated miRNAs and their abundance. M-R) Heatmap of Top 5 miRNAs from panels G-L.

Figure 3: IPA Pathway analysis of m^6A methylation of basal ganglia miRNAs: A) Neuroinflammation network molecules associated with the with miRNAs with m^6A hypomethylation (left) or hypermethylation (right). B) Two-way Venny of top 35 network molecules between the hypomethylated and hypermethylated miRNA within each animal groups. C) Three-way Venny of top 30 network molecules comparing m^6A hypomethylated versus hypermethylated miRNA irrespective of animal groups.

Figure 4: Geneontology (GO) analysis illustrating biological processes, cellular components, and molecular functions of the neuroinflammation network molecules for each animal with m^6A: A) hypomethylated and B) hyper methylated miRNA.

Figure 5: Basal ganglia miRNA with significant m^6A modifications have altered expression levels. A) Correlation analysis of m^6A methylation versus miRNA abundance. C-H) Functional relationship of m^6A methylated miRNA with neurotransmitters/other nervous system and pathogen influenced signaling pathways. I-N) PPI networks for the IPA identified miRNA targets in panels C-H.

Figure 6: THC:CBD administration significantly reduced the incorporation of m^6A epitranscriptomic marks on neuroinflammation targeting miRNAs that were increased by HIV/SIV infection: A) Heatmap of 44 miRNAs with significant m^6A hypermethylation in the VEH/SIV/cART RMs relative to THC:CBD/SIV/cART group. **B**) IPA network interactome and associated canonical signaling pathways and biological functions. **C**) Key biological processes, cellular components, and molecular functions regulated by 44 m^6A hypermethylated miRNAs. **D**) IPA network of canonical signaling pathways and functions associated with 14 miRNAs with RRACH or DRACH motif.

Figure 7: Identification of tissue-EV miRNA with m6A modification: A) 3-way Venn diagram identifying m^6A modified tissue miRNA present in EVs. B) Top 5 miRNAs in EVs. C) Top 5 miRNAs in tissues. C) Functional relationship of EV-Tissue miRNA with neurotransmitters/other nervous system and pathogen influenced signaling pathways. E) PPI networks for the IPA identified EV-Tissue miRNA targets in panels D. F) Volcano plot of biological/functional insights for EV-Tissue miRNA target gene sets.

Supplemental Figure 1: IPA Pathway analysis of m^6A methylation of basal ganglia miRNAs: A) Neuroinflammation network molecules associated with the with miRNAs with m6A hypomethylation (left) or hypermethylation (right).

Supplemental Figure 2: Correlation analysis of m^6A methylation versus miRNA abundance:

Supplemental Figure 3: Web Gestalt analysis for A) KEGG, **B)** Reactome, **C)** Diseases.

Supplemental Figure 4: miR-194-5p levels and bioinformatics analysis: A) miR-194-5p levels. **B**) miR-194-5p-STAT1 pairing.

References

1. Eden A, Fuchs D, Hagberg L, Nilsson S, Spudich S, Svennerholm B, Price RW, Gisslen M. HIV-1 viral escape in cerebrospinal fluid of subjects on suppressive antiretroviral treatment. J Infect Dis. 2010;202(12):1819-25. Epub 2010/11/06. doi: 10.1086/657342. PubMed PMID: 21050119; PMCID: 3052942.
2. Lamers SL, Gray RR, Salemi M, Huysentruyt LC, McGrath MS. HIV-1 phylogenetic analysis shows HIV-1 transits through the meninges to brain and peripheral tissues. Infect Genet Evol. 2011;11(1):31-7. Epub 2010/11/09. doi: 10.1016/j.meegid.2010.10.016. PubMed PMID: 21055482; PMCID: 3005076.
3. Spudich S, Lollo N, Liegler T, Deeks SG, Price RW. Treatment benefit on cerebrospinal fluid HIV-1 levels in the setting of systemic virological suppression and failure. J Infect Dis. 2006;194(12):1686-96. Epub 2006/11/17. doi: 10.1086/508750. PubMed PMID: 17109340.
4. Grant I, Atkinson JH, Hesselink JR, Kennedy CJ, Richman DD, Spector SA, McCutchan JA. Evidence for early central nervous system involvement in the acquired immunodeficiency syndrome (AIDS) and other human immunodeficiency virus (HIV) infections. Studies with neuropsychologic testing and magnetic resonance imaging. Ann Intern Med. 1987;107(6):828-36. Epub 1987/12/01. PubMed PMID: 3688675.
5. Sacktor N, Skolasky RL, Seaberg E, Munro C, Becker JT, Martin E, Ragin A, Levine A, Miller E. Prevalence of HIV-associated neurocognitive disorders in the Multicenter AIDS Cohort Study. Neurology. 2016;86(4):334-40. Epub 2016/01/01. doi: 10.1212/WNL.0000000000002277. PubMed PMID: 26718568; PMCID: PMC4776086.
6. Fuster-RuizdeApodaca MJ, Castro-Granell V, Garin N, Laguía A, Jaén Á, Iniesta C, Cenoz S, Galindo MJ. Prevalence and patterns of illicit drug use in people living with HIV in Spain: A cross-sectional study. PLoS One. 2019;14(6):e0211252. Epub 2019/06/18. doi: 10.1371/journal.pone.0211252. PubMed PMID: 31206550; PMCID: PMC6576760 Healthcare was involved in the study design and preparation of the manuscript, without influencing the data collection and analysis or the decision to publish. All listed authors meet the criteria for authorship set forth by the International Committee of Medical Journal Editors. All authors had full access to the data and are responsible for the veracity and completeness of the reported data. SC is employed full time in ViiV Healthcare. MJFRA, AJ, CI and MJG are members of the Spanish Interdisciplinary Aids Society (SEISIDA) Executive Board. SEISIDA has received grants from MSD, ViiV, Janssen, and Gilead. MJFRA has provided consultancy services to ViiV, Gilead, and Janssen, and have received payments for lectures or educational presentations from MSD, Gilead, and ViiV. MJG has provided consultancy services to ViiV, Abbie, MSD, Gilead, and Janssen, and has received payments for travelling to meetings from MSD and for lectures or educational presentations from MSD, Janssen, Gilead, and ViiV. CI has received payments for consultancy services to MSD.
7. Castro FOF, Silva JM, Dorneles GP, Barros JBS, Ribeiro CB, Noronha I, Barbosa GR, Souza LCS, Guilarde AO, Pereira A, Guimarães RF, Oliveira TF, Oliveira SEF, Peres A, Romão PRT, Pfrimer IAH, Fonseca SGD. Distinct inflammatory profiles in HIV-infected individuals under antiretroviral therapy using cannabis, cocaine or cannabis plus cocaine. Aids. 2019;33(12):1831-42. Epub 2019/09/07. doi: 10.1097/qad.0000000000002296. PubMed PMID: 31490211.
8. Galaj E, Bi GH, Yang HJ, Xi ZX. Cannabidiol attenuates the rewarding effects of cocaine in rats by CB2, 5-HT(1A) and TRPV1 receptor mechanisms. Neuropharmacology. 2020;167:107740. Epub 2019/08/23. doi: 10.1016/j.neuropharm.2019.107740. PubMed PMID: 31437433; PMCID: PMC7493134.
9. Mimiaga MJ, Reisner SL, Grasso C, Crane HM, Safren SA, Kitahata MM, Schumacher JE, Mathews WC, Mayer KH. Substance use among HIV-infected patients engaged in primary care in the United States: findings from the Centers for AIDS Research Network of Integrated Clinical Systems cohort. Am J Public Health. 2013;103(8):1457-67. Epub 2013/06/15. doi: 10.2105/ajph.2012.301162. PubMed PMID: 23763417; PMCID: PMC3752382.
10. Mohammadi A, Darabi M, Nasry M, Saabet-Jahromi MJ, Malek-Pour-Afshar R, Sheibani H. Effect of opium addiction on lipid profile and atherosclerosis formation in hypercholesterolemic rabbits. Exp Toxicol Pathol. 2009;61(2):145-9. Epub 2008/10/08. doi: 10.1016/j.etp.2008.08.001. PubMed PMID: 18838257.
11. Roohafza H, Talaei M, Sadeghi M, Haghani P, Shokouh P, Sarrafzadegan N. Opium decreases the age at myocardial infarction and sudden cardiac death: a long- and short-term outcome evaluation. Arch Iran Med. 2013;16(3):154-60. Epub 2013/02/26. doi: 013163/aim.007. PubMed PMID: 23432167.
12. Nabati S, Asadikaram G, Arababadi MK, Shahabinejad G, Rezaeian M, Mahmoodi M, Kennedy D. The plasma levels of the cytokines in opium-addicts and the effects of opium on the cytokines secretion by their

lymphocytes. Immunol Lett. 2013;152(1):42-6. Epub 2013/04/23. doi: 10.1016/j.imlet.2013.04.003. PubMed PMID: 23603301.
13. Saha B, Momen-Heravi F, Kodys K, Szabo G. MicroRNA Cargo of Extracellular Vesicles from Alcohol-exposed Monocytes Signals Naive Monocytes to Differentiate into M2 Macrophages. J Biol Chem. 2016;291(1):149-59. Epub 2015/11/04. doi: 10.1074/jbc.M115.694133. PubMed PMID: 26527689; PMCID: PMC4697152.
14. Momen-Heravi F, Saha B, Kodys K, Catalano D, Satishchandran A, Szabo G. Increased number of circulating exosomes and their microRNA cargos are potential novel biomarkers in alcoholic hepatitis. J Transl Med. 2015;13:261. Epub 2015/08/13. doi: 10.1186/s12967-015-0623-9. PubMed PMID: 26264599; PMCID: PMC4533956.
15. Momen-Heravi F, Bala S, Kodys K, Szabo G. Exosomes derived from alcohol-treated hepatocytes horizontally transfer liver specific miRNA-122 and sensitize monocytes to LPS. Sci Rep. 2015;5:9991. Epub 2015/05/15. doi: 10.1038/srep09991. PubMed PMID: 25973575; PMCID: PMC4650752.
16. McDew-White M, Lee E, Alvarez X, Sestak K, Ling BJ, Byrareddy SN, Okeoma CM, Mohan M. Cannabinoid control of gingival immune activation in chronically SIV-infected rhesus macaques involves modulation of the indoleamine-2,3-dioxygenase-1 pathway and salivary microbiome. EBioMedicine. 2022;75:103769. Epub 2021/12/27. doi: 10.1016/j.ebiom.2021.103769. PubMed PMID: 34954656; PMCID: PMC8715300.
17. McDew-White M, Lee E, Premadasa LS, Alvarez X, Okeoma CM, Mohan M. Cannabinoids modulate the microbiota-gut-brain axis in HIV/SIV infection by reducing neuroinflammation and dysbiosis while concurrently elevating endocannabinoid and indole-3-propionate levels. J Neuroinflammation. 2023;20(1):62. Epub 2023/03/09. doi: 10.1186/s12974-023-02729-6. PubMed PMID: 36890518; PMCID: PMC9993397.
18. Kaddour H, McDew-White M, Madeira MM, Tranquille MA, Tsirka SE, Mohan M, Okeoma CM. Chronic delta-9-tetrahydrocannabinol (THC) treatment counteracts SIV-induced modulation of proinflammatory microRNA cargo in basal ganglia-derived extracellular vesicles. J Neuroinflammation. 2022;19(1):225. Epub 2022/09/13. doi: 10.1186/s12974-022-02586-9. PubMed PMID: 36096938; PMCID: PMC9469539.
19. Jonkhout N, Tran J, Smith MA, Schonrock N, Mattick JS, Novoa EM. The RNA modification landscape in human disease. RNA. 2017;23(12):1754-69. Epub 2017/09/01. doi: 10.1261/rna.063503.117. PubMed PMID: 28855326; PMCID: PMC5688997.
20. Fan Y, Lv X, Chen Z, Peng Y, Zhang M. m6A methylation: Critical roles in aging and neurological diseases. Front Mol Neurosci. 2023;16:1102147. Epub 2023/03/11. doi: 10.3389/fnmol.2023.1102147. PubMed PMID: 36896007; PMCID: PMC9990872.
21. Zhang F, Ran Y, Tahir M, Li Z, Wang J, Chen X. Regulation of N6-methyladenosine (m6A) RNA methylation in microglia-mediated inflammation and ischemic stroke. Front Cell Neurosci. 2022;16:955222. Epub 2022/08/23. doi: 10.3389/fncel.2022.955222. PubMed PMID: 35990887; PMCID: PMC9386152.
22. Chatterjee B, Shen CJ, Majumder P. RNA Modifications and RNA Metabolism in Neurological Disease Pathogenesis. Int J Mol Sci. 2021;22(21). Epub 2021/11/14. doi: 10.3390/ijms222111870. PubMed PMID: 34769301; PMCID: PMC8584444.
23. Hill M, Tran N. Global miRNA to miRNA Interactions: Impacts for miR-21. Trends Cell Biol. 2021;31(1):3-5. Epub 20201111. doi: 10.1016/j.tcb.2020.10.005. PubMed PMID: 33189493.
24. Ooi JYY, Bernardo BC, Singla S, Patterson NL, Lin RCY, McMullen JR. Identification of miR-34 regulatory networks in settings of disease and antimiR-therapy: Implications for treating cardiac pathology and other diseases. RNA Biol. 2017;14(5):500-13. Epub 20160428. doi: 10.1080/15476286.2016.1181251. PubMed PMID: 27124358; PMCID: PMC5449084.
25. Wang D, Sun X, Wei Y, Liang H, Yuan M, Jin F, Chen X, Liu Y, Zhang CY, Li L, Zen K. Nuclear miR-122 directly regulates the biogenesis of cell survival oncomiR miR-21 at the posttranscriptional level. Nucleic Acids Res. 2018;46(4):2012-29. doi: 10.1093/nar/gkx1254. PubMed PMID: 29253196; PMCID: PMC5829740.
26. Price AM, Hayer KE, McIntyre ABR, Gokhale NS, Abebe JS, Della Fera AN, Mason CE, Horner SM, Wilson AC, Depledge DP, Weitzman MD. Direct RNA sequencing reveals m(6)A modifications on adenovirus RNA are necessary for efficient splicing. Nat Commun. 2020;11(1):6016. Epub 2020/11/28. doi: 10.1038/s41467-020-19787-6. PubMed PMID: 33243990; PMCID: PMC7691994 as an advisor or compensated speaker for Abbvie, Acuamark Diagnostics, ArcBio, BioRad, DNA Genotek, Genialis, Genpro, Karius, Illumina, New England Biolabs, QIAGEN, Whole Biome, and Zymo Research. The remaining authors declare no competing interests.

27. Kashima R, Hata A. The role of TGF-beta superfamily signaling in neurological disorders. Acta Biochim Biophys Sin (Shanghai). 2018;50(1):106-20. Epub 2017/12/01. doi: 10.1093/abbs/gmx124. PubMed PMID: 29190314; PMCID: PMC5846707.
28. Su C, Miao J, Guo J. The relationship between TGF-beta1 and cognitive function in the brain. Brain Res Bull. 2023;205:110820. Epub 2023/11/19. doi: 10.1016/j.brainresbull.2023.110820. PubMed PMID: 37979810.
29. Deng Z, Fan T, Xiao C, Tian H, Zheng Y, Li C, He J. TGF-beta signaling in health, disease, and therapeutics. Signal Transduct Target Ther. 2024;9(1):61. Epub 2024/03/22. doi: 10.1038/s41392-024-01764-w. PubMed PMID: 38514615; PMCID: PMC10958066.
30. Cooper DB, Bunner AE, Kennedy JE, Balldin V, Tate DF, Eapen BC, Jaramillo CA. Treatment of persistent post-concussive symptoms after mild traumatic brain injury: a systematic review of cognitive rehabilitation and behavioral health interventions in military service members and veterans. Brain Imaging Behav. 2015;9(3):403-20. Epub 2015/09/04. doi: 10.1007/s11682-015-9440-2. PubMed PMID: 26330376.
31. Russo E, Guy GW. A tale of two cannabinoids: the therapeutic rationale for combining tetrahydrocannabinol and cannabidiol. Med Hypotheses. 2006;66(2):234-46. Epub 2005/10/08. doi: 10.1016/j.mehy.2005.08.026. PubMed PMID: 16209908.
32. Vermersch P. Sativex(®) (tetrahydrocannabinol + cannabidiol), an endocannabinoid system modulator: basic features and main clinical data. Expert Rev Neurother. 2011;11(4 Suppl):15-9. Epub 2011/04/01. doi: 10.1586/ern.11.27. PubMed PMID: 21449855.
33. Wang H, Song X, Song C, Wang X, Cao H. m(6)A-seq analysis of microRNAs reveals that the N6-methyladenosine modification of miR-21-5p affects its target expression. Arch Biochem Biophys. 2021;711:109023. Epub 20210901. doi: 10.1016/j.abb.2021.109023. PubMed PMID: 34480914.
34. Roberts ES, Burudi EM, Flynn C, Madden LJ, Roinick KL, Watry DD, Zandonatti MA, Taffe MA, Fox HS. Acute SIV infection of the brain leads to upregulation of IL6 and interferon-regulated genes: expression patterns throughout disease progression and impact on neuroAIDS. J Neuroimmunol. 2004;157(1-2):81-92. doi: 10.1016/j.jneuroim.2004.08.030. PubMed PMID: 15579284.
35. Berulava T, Rahmann S, Rademacher K, Klein-Hitpass L, Horsthemke B. N6-adenosine methylation in MiRNAs. PloS one. 2015;10(2):e0118438. Epub 20150227. doi: 10.1371/journal.pone.0118438. PubMed PMID: 25723394; PMCID: PMC4344304.
36. van den Homberg DAL, van der Kwast R, Quax PHA, Nossent AY. N-6-Methyladenosine in Vasoactive microRNAs during Hypoxia; A Novel Role for METTL4. Int J Mol Sci. 2022;23(3). Epub 20220119. doi: 10.3390/ijms23031057. PubMed PMID: 35162982; PMCID: PMC8835077.
37. Lichinchi G, Gao S, Saletore Y, Gonzalez GM, Bansal V, Wang Y, Mason CE, Rana TM. Dynamics of the human and viral m(6)A RNA methylomes during HIV-1 infection of T cells. Nat Microbiol. 2016;1:16011. Epub 20160222. doi: 10.1038/nmicrobiol.2016.11. PubMed PMID: 27572442; PMCID: PMC6053355.
38. Lichinchi G, Rana TM. Profiling of N(6)-Methyladenosine in Zika Virus RNA and Host Cellular mRNA. Methods Mol Biol. 2019;1870:209-18. doi: 10.1007/978-1-4939-8808-2_16. PubMed PMID: 30539558.
39. Lichinchi G, Zhao BS, Wu Y, Lu Z, Qin Y, He C, Rana TM. Dynamics of Human and Viral RNA Methylation during Zika Virus Infection. Cell Host Microbe. 2016;20(5):666-73. Epub 20161020. doi: 10.1016/j.chom.2016.10.002. PubMed PMID: 27773536; PMCID: PMC5155635.
40. Platanias LC. Mechanisms of type-I- and type-II-interferon-mediated signalling. Nat Rev Immunol. 2005;5(5):375-86. doi: 10.1038/nri1604. PubMed PMID: 15864272.

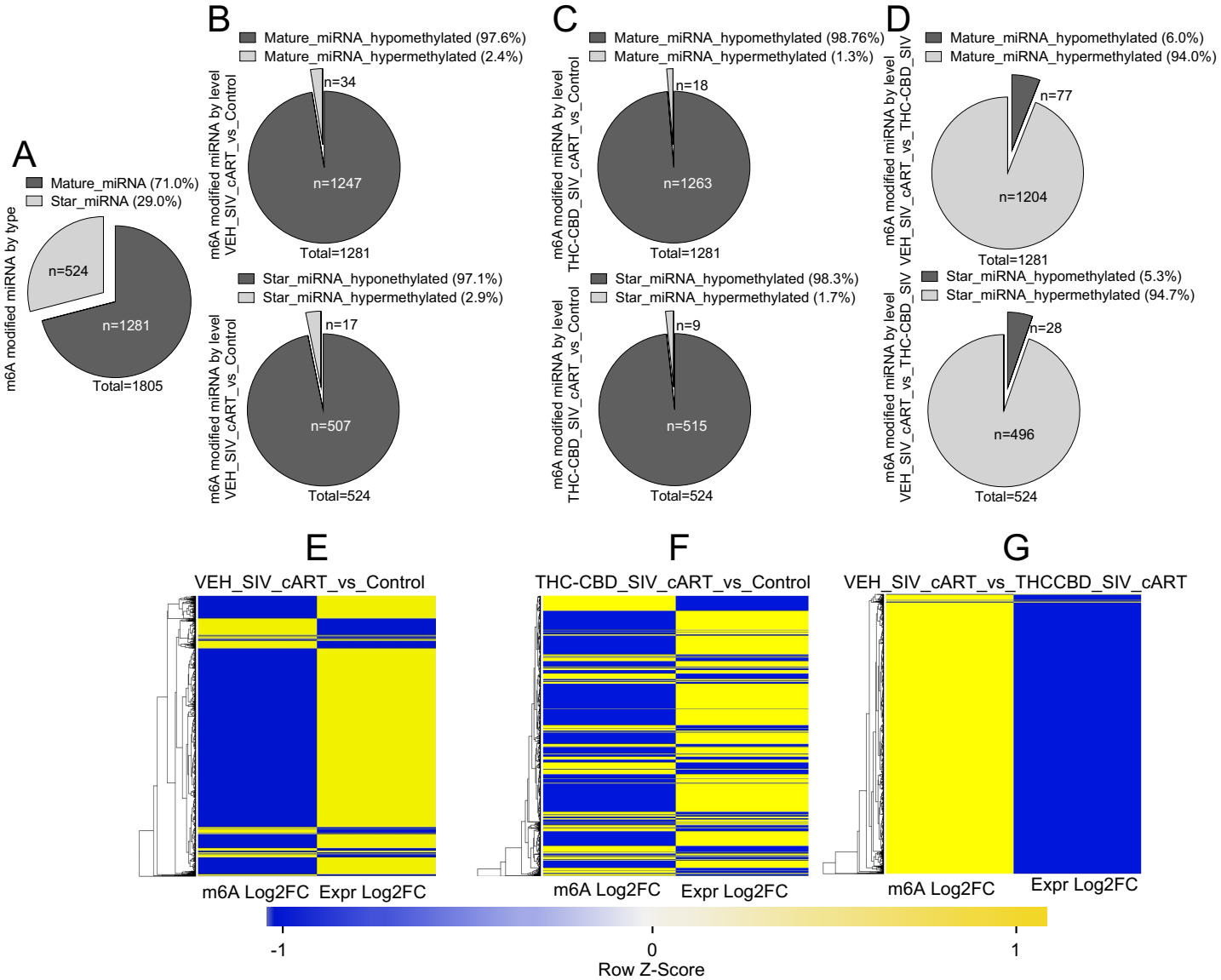
A
m6A modified miRNA by type
Mature_miRNA (71.0%)
Star_miRNA (29.0%)
n=524
n=1281
Total=1805
B
m6A modified miRNA by level
VEH_SIV_cART_vs_Control
Mature_miRNA_hypomethylated (97.6%)
Mature_miRNA_hypermethylated (2.4%)
n=34
n=1247
Total=1281
Star_miRNA_hyponethylated (97.1%)
Star_miRNA_hypermethylated (2.9%)
n=17
n=507
Total=524
C
m6A modified miRNA by level
THC-CBD_SIV_cART_vs_Control
Mature_miRNA_hypomethylated (98.76%)
Mature_miRNA_hypermethylated (1.3%)
n=18
n=1263
Total=1281
Star_miRNA_hypomethylated (98.3%)
Star_miRNA_hypermethylated (1.7%)
n=9
n=515
Total=524
D
m6A modified miRNA by level
VEH_SIV_cART_vs_THC-CBD_SIV
Mature_miRNA_hypomethylated (6.0%)
Mature_miRNA_hypermethylated (94.0%)
n=77
n=1204
Total=1281
Star_miRNA_hypomethylated (5.3%)
Star_miRNA_hypermethylated (94.7%)
n=28
n=496
Total=524
E
VEH_SIV_cART_vs_Control
m6A Log2FC
Expr Log2FC
F
THC-CBD_SIV_cART_vs_Control
m6A Log2FC
Expr Log2FC
G
VEH_SIV_cART_vs_THCCBD_SIV_cART
m6A Log2FC
Expr Log2FC
-1
0
1
Row Z-Score

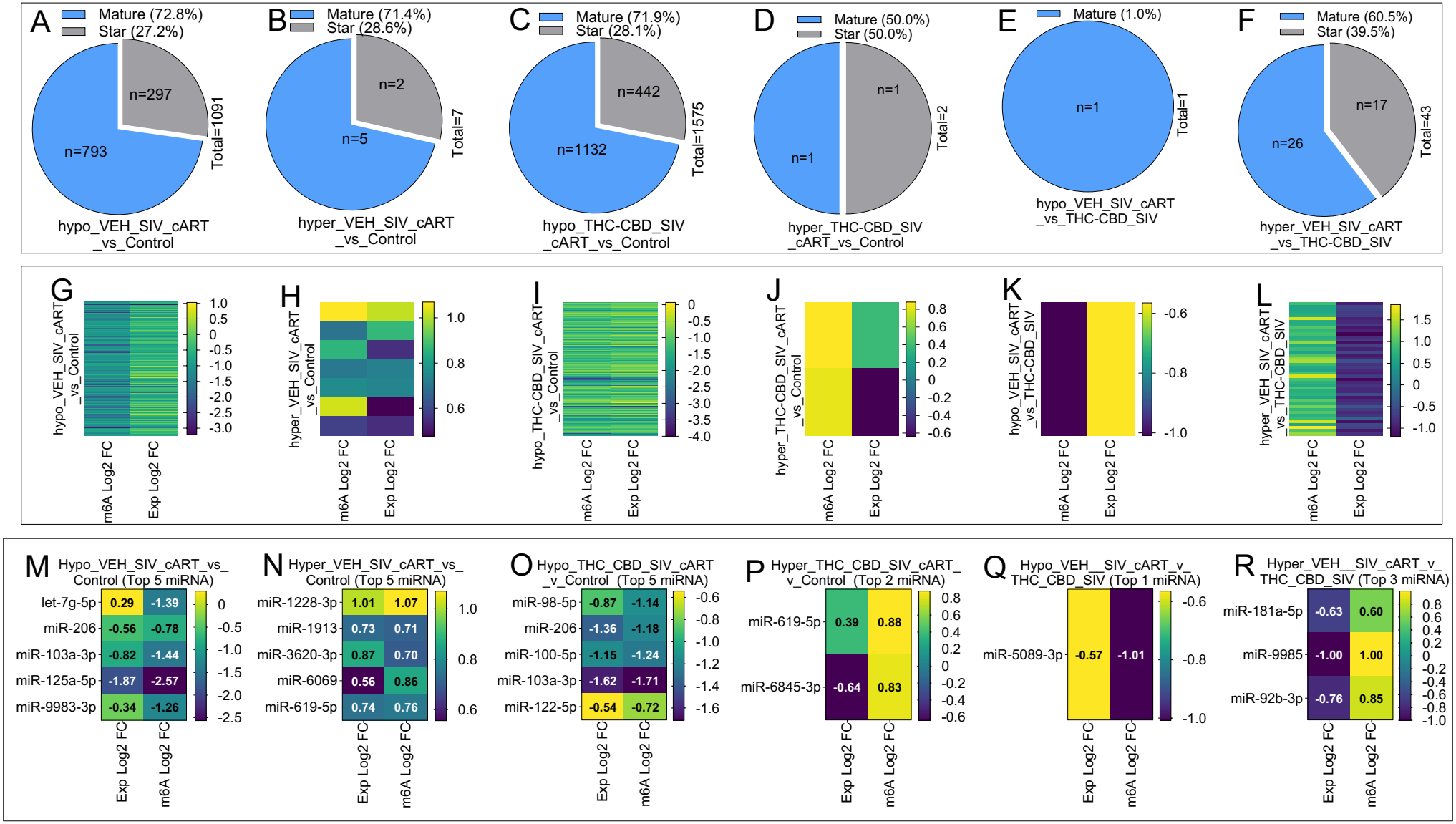
A
Mature (72.8%)
Star (27.2%)
n=297
n=793
Total=1091
hypo_VEH_SIV_cART _vs_Control
B
Mature (71.4%)
Star (28.6%)
n=2
n=5
Total=7
hyper_VEH_SIV_cART _vs_Control
C
Mature (71.9%)
Star (28.1%)
n=442
n=1132
Total=1575
hypo_THC-CBD_SIV _cART_vs_Control
D
Mature (50.0%)
Star (50.0%)
n=1
n=1
Total=2
hyper_THC-CBD_SIV _cART_vs_Control
E
Mature (1.0%)
n=1
Total=1
hypo_VEH_SIV_cART _vs_THC-CBD_SIV
F
Mature (60.5%)
Star (39.5%)
n=17
n=26
Total=43
hyper_VEH_SIV_cART _vs_THC-CBD_SIV
G
hypo_VEH_SIV_cART _vs_Control
m6A Log2 FC
Exp Log2 FC
H
hyper_VEH_SIV_cART _vs_Control
m6A Log2 FC
Exp Log2 FC
I
hypo_THC-CBD_SIV_cART _vs_Control
m6A Log2 FC
Exp Log2 FC
J
hyper_THC-CBD_SIV_cART _vs_Control
m6A Log2 FC
Exp Log2 FC
K
hypo_VEH_SIV_cART _vs_THC-CBD_SIV
m6A Log2 FC
Exp Log2 FC
L
hyper_VEH_SIV_cART _vs_THC-CBD_SIV
m6A Log2 FC
Exp Log2 FC
M
Hypo_VEH_SIV_cART_vs_ Control (Top 5 miRNA)
let-7g-5p 0.29 -1.39
miR-206 -0.56 -0.78
miR-103a-3p -0.82 -1.44
miR-125a-5p -1.87 -2.57
miR-9983-3p -0.34 -1.26
Exp Log2 FC
m6A Log2 FC
N
Hyper_VEH_SIV_cART_vs_ Control (Top 5 miRNA)
miR-1228-3p 1.01 1.07
miR-1913 0.73 0.71
miR-3620-3p 0.87 0.70
miR-6069 0.56 0.86
miR-619-5p 0.74 0.76
Exp Log2 FC
m6A Log2 FC
O
Hypo_THC_CBD_SIV_cART _v_Control (Top 5 miRNA)
miR-98-5p -0.87 -1.14
miR-206 -1.36 -1.18
miR-100-5p -1.15 -1.24
miR-103a-3p -1.62 -1.71
miR-122-5p -0.54 -0.72
Exp Log2 FC
m6A Log2 FC
P
Hyper_THC_CBD_SIV_cART_ v_Control (Top 2 miRNA)
miR-619-5p 0.39 0.88
miR-6845-3p -0.64 0.83
Exp Log2 FC
m6A Log2 FC
Q
Hypo_VEH__SIV_cART_v_ THC_CBD_SIV (Top 1 miRNA)
miR-5089-3p -0.57 -1.01
Exp Log2 FC
m6A Log2 FC
R
Hyper_VEH__SIV_cART_v_ THC_CBD_SIV (Top 3 miRNA)
miR-181a-5p -0.63 0.60
miR-9985 -1.00 1.00
miR-92b-3p -0.76 0.85
Exp Log2 FC
m6A Log2 FC

Neuroinflammation networks

A

m6A hypomethylation

VEH_SIV_cART_vs_Control

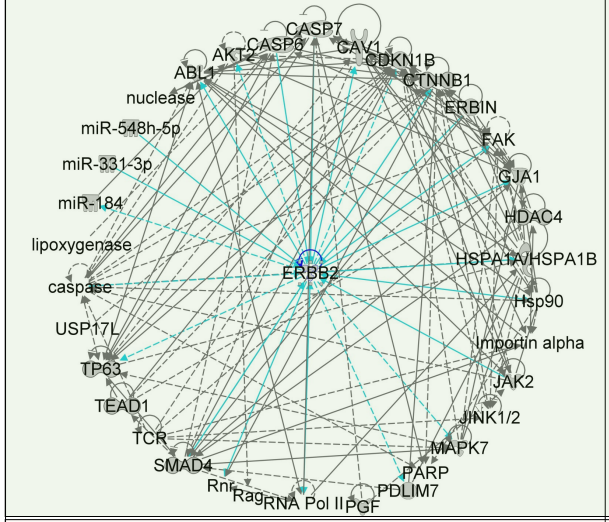

THC-CBD_SIV_cART_vs_Control

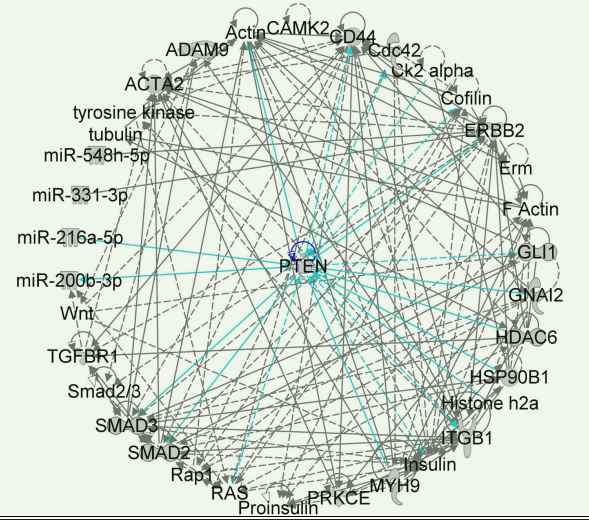

VEH_SIV_cART_vs_THC-CBD_SIV

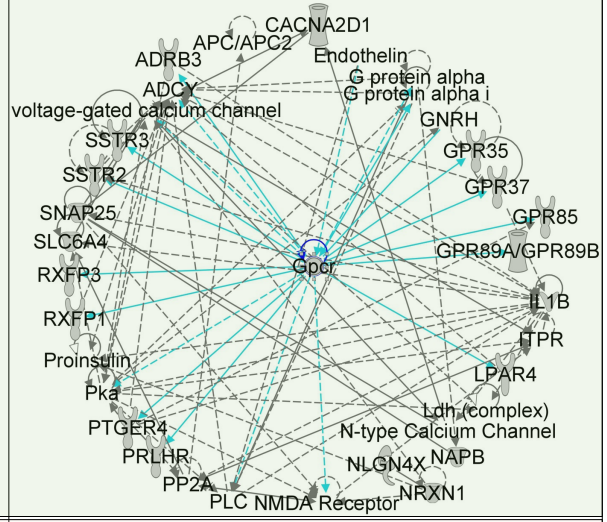

B

m6A hypermethylation

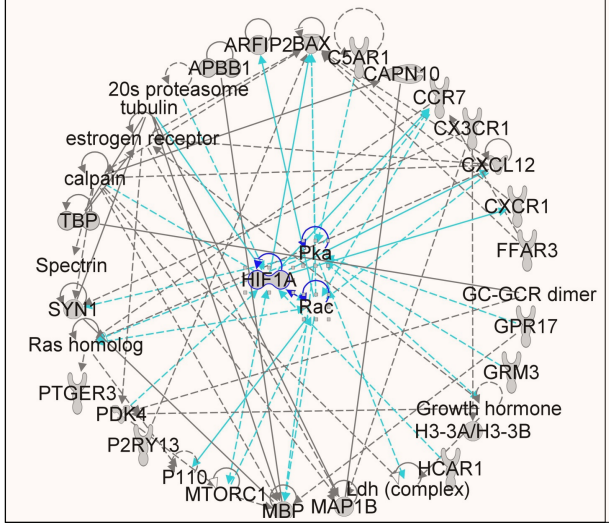

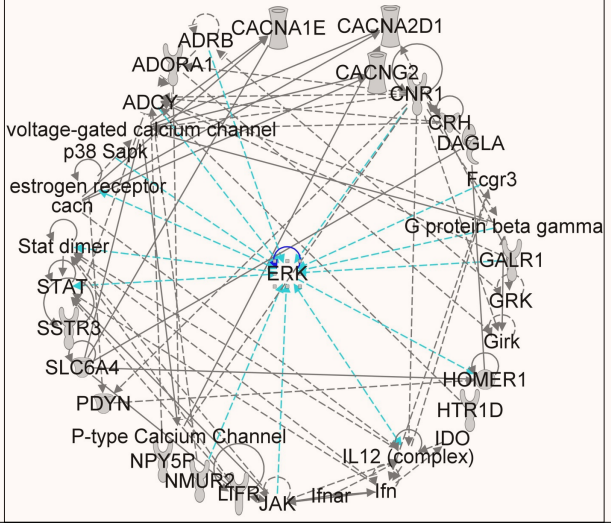

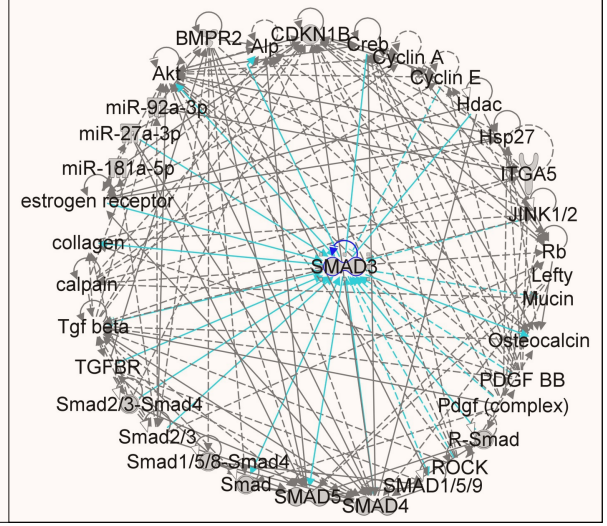

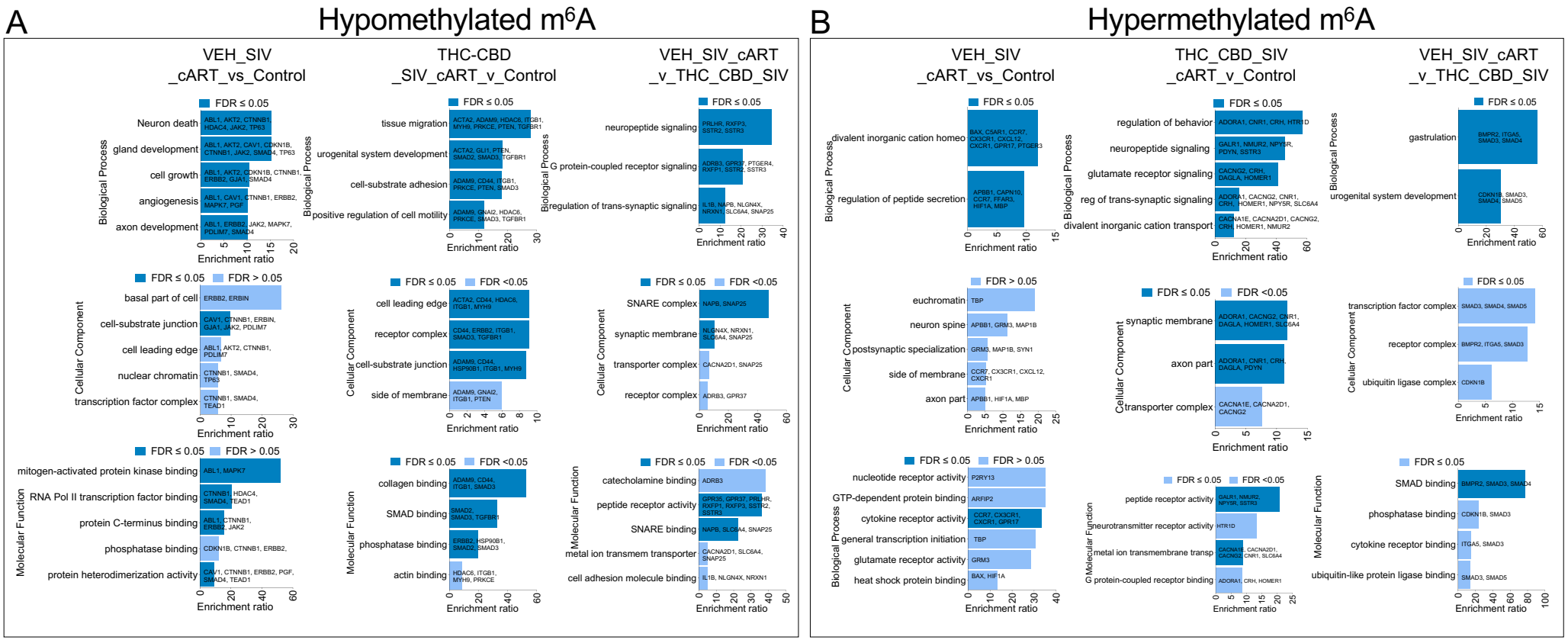
A
Hypomethylated m6A
VEH_SIV _cART_vs_Control
THC-CBD _SIV_cART_v_Control
VEH_SIV_cART _v_THC_CBD_SIV
FDR ≤ 0.05
Biological Process
Neuron death
gland development
cell growth
angiogenesis
axon development
tissue migration
urogenital system development
cell-substrate adhesion
positive regulation of cell motility
neuropeptide signaling
G protein-coupled receptor signaling
regulation of trans-synaptic signaling
Enrichment ratio
FDR > 0.05
FDR <0.05
Cellular Component
basal part of cell
cell-substrate junction
cell leading edge
nuclear chromatin
transcription factor complex
receptor complex
side of membrane
SNARE complex
synaptic membrane
transporter complex
Molecular Function
mitogen-activated protein kinase binding
RNA Pol II transcription factor binding
protein C-terminus binding
phosphatase binding
protein heterodimerization activity
collagen binding
SMAD binding
actin binding
catecholamine binding
peptide receptor activity
SNARE binding
metal ion transmem transporter
cell adhesion molecule binding
B
Hypermethylated m6A
VEH_SIV _cART_vs_Control
THC_CBD_SIV _cART_v_Control
VEH_SIV_cART _v_THC_CBD_SIV
divalent inorganic cation homeo
regulation of peptide secretion
regulation of behavior
neuropeptide signaling
glutamate receptor signaling
reg of trans-synaptic signaling
divalent inorganic cation transport
gastrulation
urogenital system development
euchromatin
neuron spine
postsynaptic specialization
side of membrane
axon part
synaptic membrane
transporter complex
transcription factor complex
receptor complex
ubiquitin ligase complex
nucleotide receptor activity
GTP-dependent protein binding
cytokine receptor activity
general transcription initiation
glutamate receptor activity
heat shock protein binding
peptide receptor activity
neurotransmitter receptor activity
metal ion transmembrane transp
G protein-coupled receptor binding
SMAD binding
phosphatase binding
cytokine receptor binding
ubiquitin-like protein ligase binding

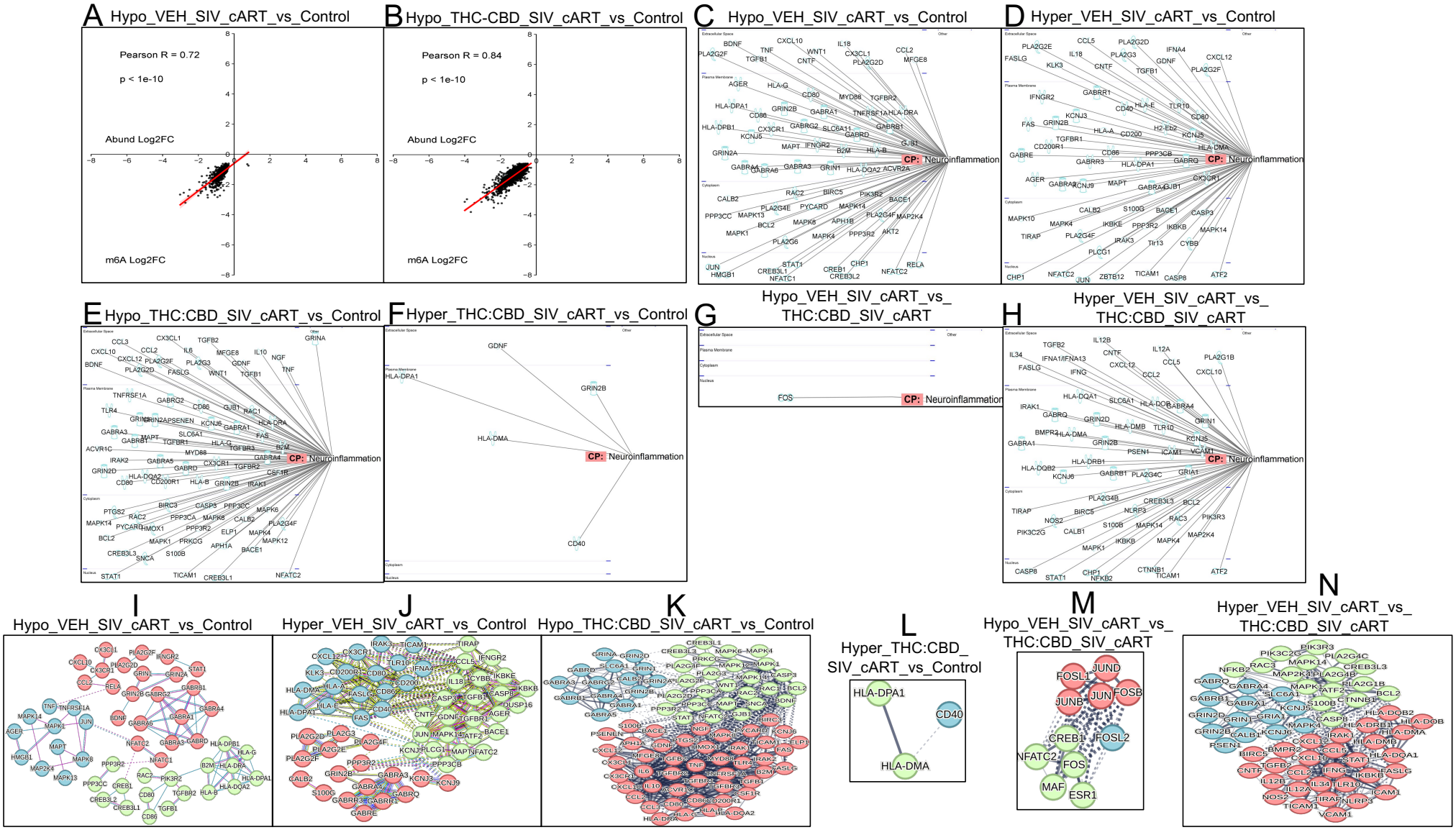
A
Hypo_VEH_SIV_cART_vs_Control
Pearson R = 0.72
p < 1e-10
Abund Log2FC
m6A Log2FC
B
Hypo_THC-CBD_SIV_cART_vs_Control
Pearson R = 0.84
p < 1e-10
Abund Log2FC
m6A Log2FC
C
Hypo_VEH_SIV_cART_vs_Control
CP: Neuroinflammation
D
Hyper_VEH_SIV_cART_vs_Control
CP: Neuroinflammation
E
Hypo_THC:CBD_SIV_cART_vs_Control
CP: Neuroinflammation
F
Hyper_THC:CBD_SIV_cART_vs_Control
CP: Neuroinflammation
G
Hypo_VEH_SIV_cART_vs_
THC:CBD_SIV_cART
CP: Neuroinflammation
H
Hyper_VEH_SIV_cART_vs_
THC:CBD_SIV_cART
CP: Neuroinflammation
I
Hypo_VEH_SIV_cART_vs_Control
J
Hyper_VEH_SIV_cART_vs_Control
K
Hypo_THC:CBD_SIV_cART_vs_Control
L
Hyper_THC:CBD_
SIV_cART_vs_Control
HLA-DPA1
CD40
HLA-DMA
M
Hypo_VEH_SIV_cART_vs_
THC:CBD_SIV_cART
FOSL1
JUND
JUNB
JUN
FOSB
CREB1
FOSL2
NFATC2
FOS
MAF
ESR1
N
Hyper_VEH_SIV_cART_vs_
THC:CBD_SIV_cART

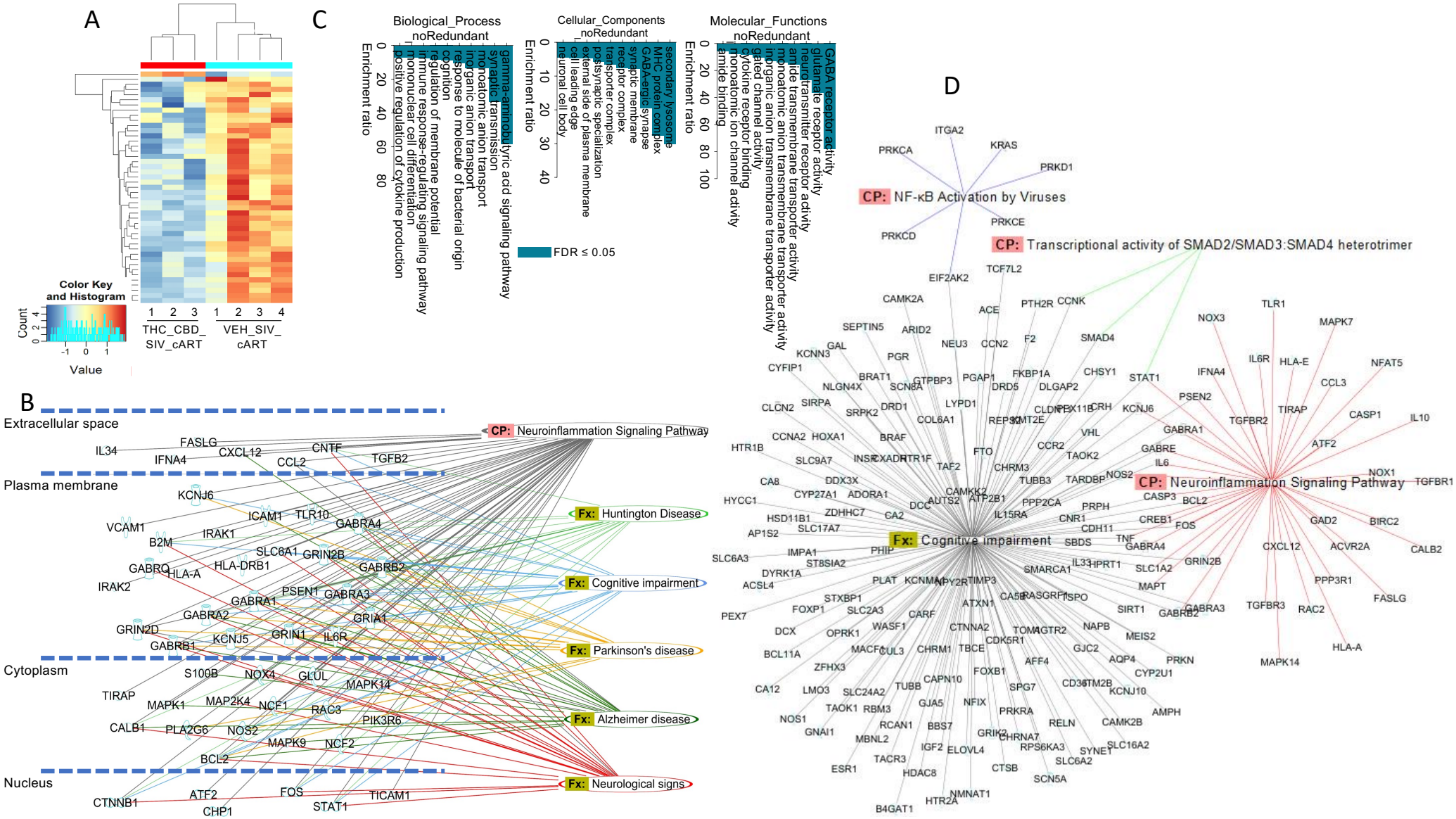
A
Color Key and Histogram
Count
Value
THC_CBD_SIV_cART
VEH_SIV_cART
C
Biological_Process_noRedundant
Cellular_Components_noRedundant
Molecular_Functions_noRedundant
Enrichment ratio
FDR ≤ 0.05
B
Extracellular space
Plasma membrane
Cytoplasm
Nucleus
CP: Neuroinflammation Signaling Pathway
Fx: Huntington Disease
Fx: Cognitive impairment
Fx: Parkinson's disease
Fx: Alzheimer disease
Fx: Neurological signs
D
CP: NF-κB Activation by Viruses
CP: Transcriptional activity of SMAD2/SMAD3:SMAD4 heterotrimer
CP: Neuroinflammation Signaling Pathway
Fx: Cognitive impairment

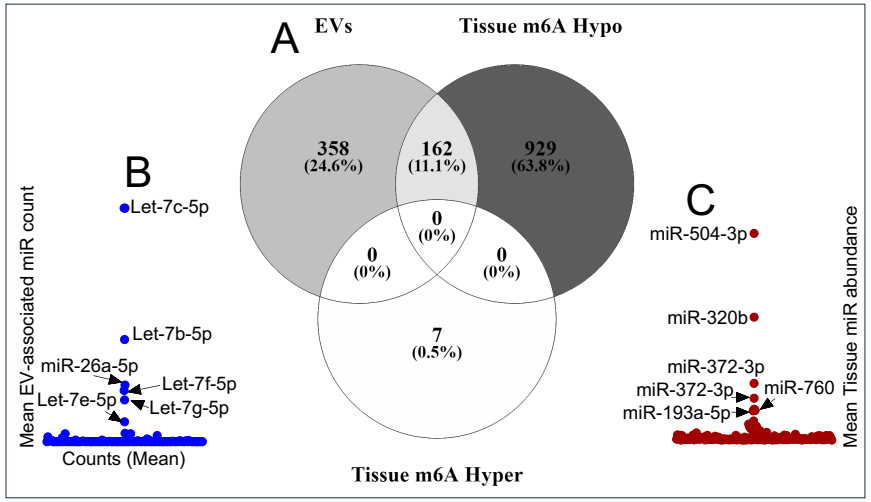
A
EVs
Tissue m6A Hypo
358
(24.6%)
162
(11.1%)
929
(63.8%)
0
(0%)
0
(0%)
0
(0%)
7
(0.5%)
Tissue m6A Hyper
B
Let-7c-5p
Let-7b-5p
miR-26a-5p
Let-7f-5p
Let-7e-5p
Let-7g-5p
Mean EV-associated miR count
Counts (Mean)
C
miR-504-3p
miR-320b
miR-372-3p
miR-372-3p
miR-760
miR-193a-5p
Mean Tissue miR abundance

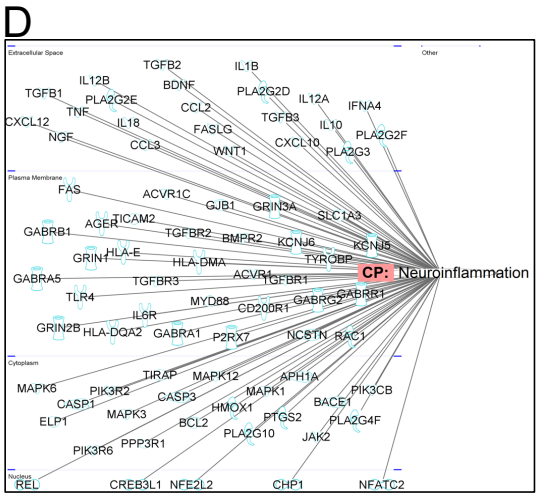
D
CP: Neuroinflammation

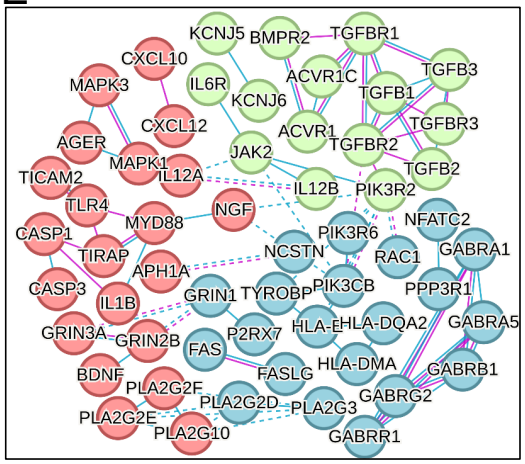
E

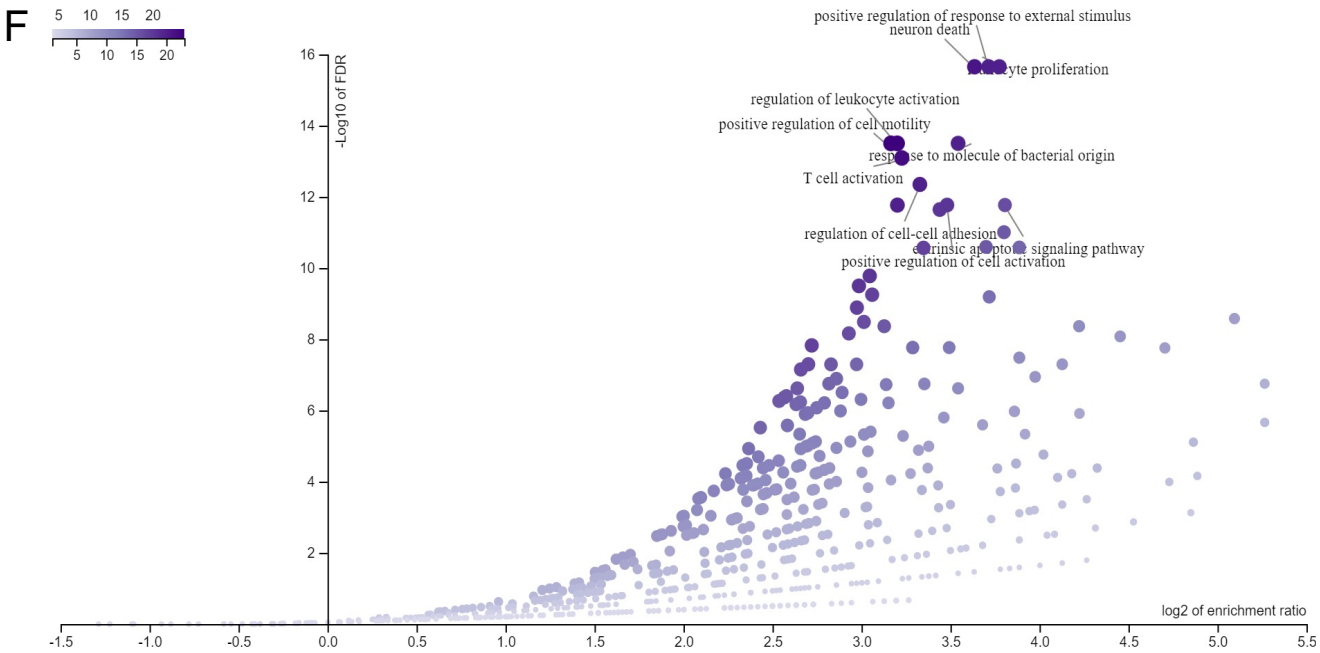
F
5 10 15 20
-Log10 of FDR
positive regulation of response to external stimulus
neuron death
regulation of leukocyte activation
positive regulation of cell motility
response to molecule of bacterial origin
T cell activation
regulation of cell-cell adhesion
extrinsic apoptotic signaling pathway
positive regulation of cell activation
log2 of enrichment ratio

Sup Fig. 1

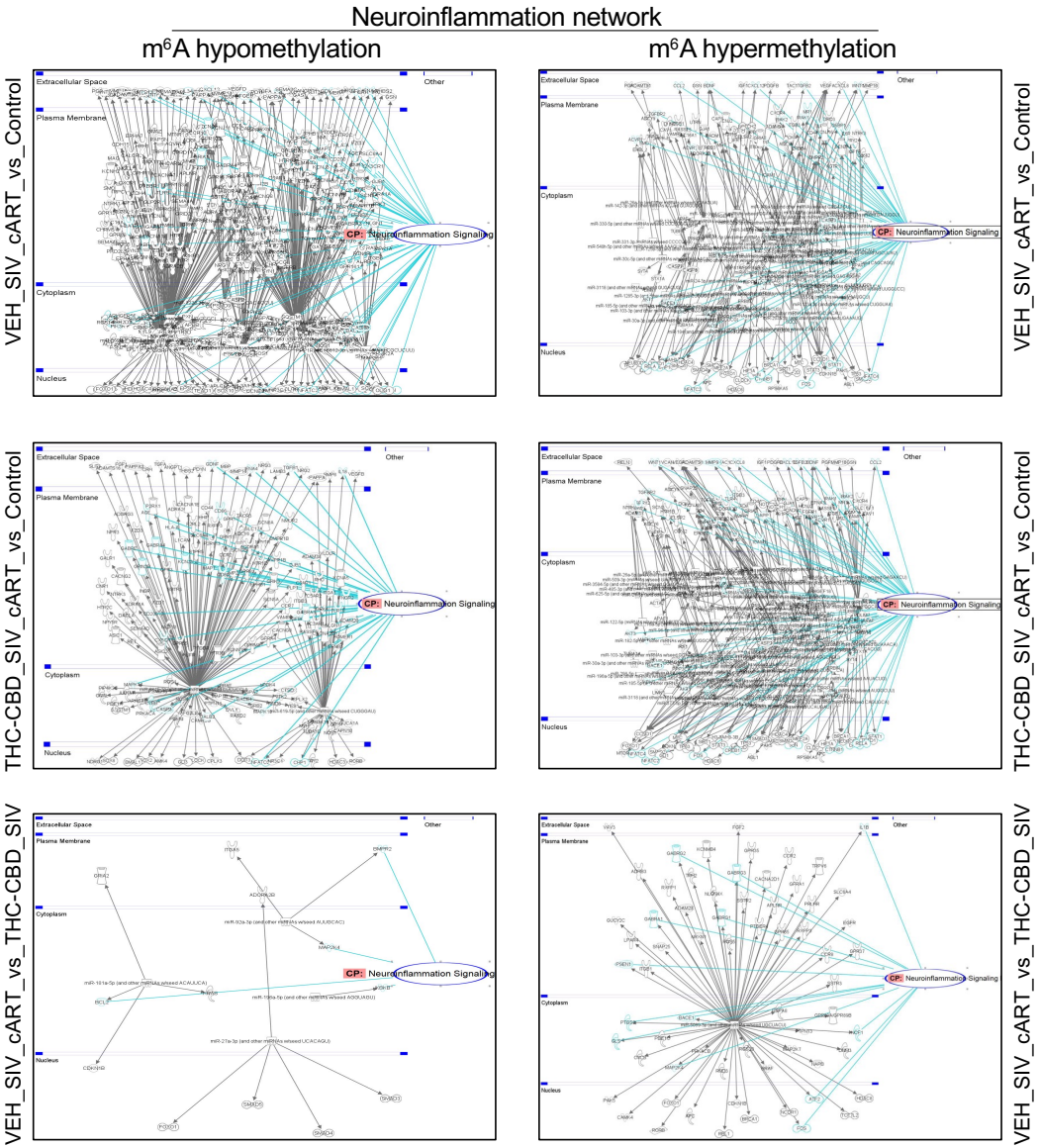
Neuroinflammation network
m6A hypomethylation
m6A hypermethylation
VEH_SIV_cART_vs_Control
THC-CBD_SIV_cART_vs_Control
VEH_SIV_cART_vs_THC-CBD_SIV
Extracellular Space
Plasma Membrane
Cytoplasm
Nucleus
Other
CP: Neuroinflammation Signaling

Sup Fig. 2

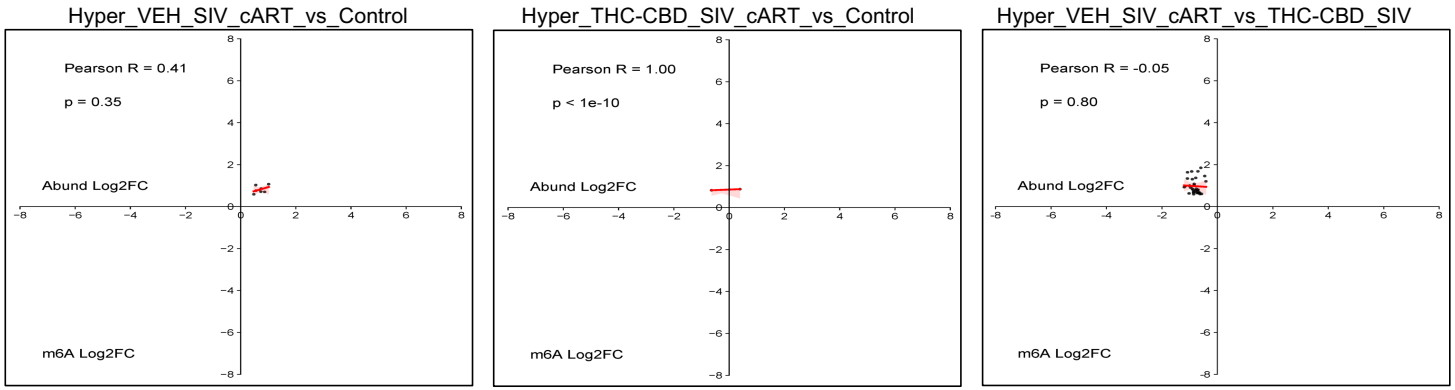
Hyper_VEH_SIV_cART_vs_Control
Pearson R = 0.41
p = 0.35
Abund Log2FC
m6A Log2FC
Hyper_THC-CBD_SIV_cART_vs_Control
Pearson R = 1.00
p < 1e-10
Abund Log2FC
m6A Log2FC
Hyper_VEH_SIV_cART_vs_THC-CBD_SIV
Pearson R = -0.05
p = 0.80
Abund Log2FC
m6A Log2FC

Sup Fig. 3

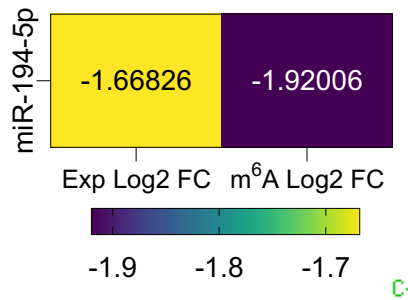

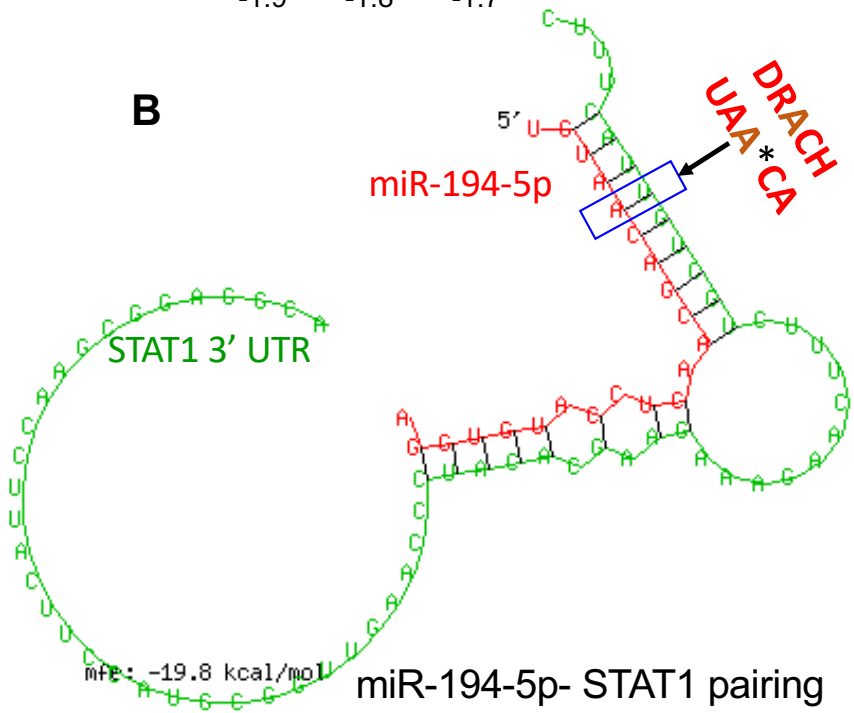

miR-194-5p- STAT1 pairing

miR-194-5p- UG***UAA*CA***GC**AACU**CCAUGUGGA (STAT1)